Investigation of the CRT performance of a PET scanner based in liquid xenon: A Monte Carlo study

J.J. Gomez-Cadenas,[a,1] J.M. Benlloch-Rodríguez,[a] P. Ferrario,[a] F. Monrabal,[b] J. Rodríguez,[a] J.F. Toledo[c]

[a]*Instituto de Física Corpuscular (IFIC), CSIC & Universitat de València,*
Calle Catedrático José Beltrán, 2, 46980 Paterna, Valencia, Spain

[b]*Department of Physics, University of Texas at Arlington*
Arlington, Texas 76019, USA

[c]*Instituto de Instrumentación para Imagen Molecular (I3M), Universitat Politècnica de València*
Camino de Vera, s/n, Edificio 8B, 46022 Valencia, Spain

E-mail: gomez@mail.cern.ch

Abstract: The measurement of the time of flight of the two 511 keV gammas recorded in coincidence in a PET scanner provides an effective way of reducing the random background and therefore increases the scanner sensitivity, provided that the coincidence resolving time (CRT) of the gammas is sufficiently good. Existing commercial systems based in LYSO crystals, such as the GEMINIS of Philips, reach CRT values of ~ 600 ps (FWHM).

In this paper we present a Monte Carlo investigation of the CRT performance of a PET scanner exploiting the scintillating properties of liquid xenon. We find that an excellent CRT of 60–70 ps (depending on the PDE of the sensor) can be obtained if the scanner is instrumented with silicon photomultipliers (SiPMs) sensitive to the ultraviolet light emitted by xenon. Alternatively, a CRT of 120 ps can be obtained instrumenting the scanner with (much cheaper) blue-sensitive SiPMs coated with a suitable wavelength shifter. These results show the excellent time of flight capabilities of a PET device based in liquid xenon.

---

[1]Corresponding author.

Contents

1 Introduction

Positron Emission Tomography (PET) is a non invasive imaging technique that produces a three-dimensional image of functional processes –it does not show anatomic features, but it rather measures the metabolic activity of the cells– in the body. PET is used in both clinical and pre-clinical research to study the molecular bases and treatments of disease. The principle of operation relies in injecting into the patient a biologically active molecule doped with a radioactive isotope, called tracer (a standard tracer is fluorodeoxyglucose, formed substituting an atom of oxygen by the isotope ^{18}F in a glucose molecule). The radionuclide decays and the resulting positrons subsequently annihilate with electrons after traveling a short distance within the subject. Each annihilation produces two 511 keV photons emitted most of the time in opposite directions and these photons are registered by a detection system. For a pair coincidence event, if the energy of two photons stays within a pre-set energy window, centred on the 511 keV photopeak, and the timing difference stays within a pre-set time window, a coincidence event will be registered and constitutes a line-of-response (LOR) for image reconstruction.

The reconstruction of the image in a PET system requires crossing many LORs which in turn define one emission point in the area under study. A LOR can be formed by: 1) a **true coincidence**, which occurs when both photons from an annihilation event are detected, neither photon undergoes any form of interaction prior to detection, and no other event is detected within the coincidence time-window; 2) a **scattered coincidence**, which occurs when one or both detected photons undergo at least one Compton scattering interaction prior to detection. Since the direction of the photon changes due to the scattering process, the resulting coincidence event will, most likely, produce a wrong LOR. Scattered coincidences add a background to the true coincidence distribution, decreasing contrast and causing the isotope concentrations to be overestimated. They also add statistical noise to the signal; 3) a **random coincidence**, which occurs when two photons, not arising from the same annihilation event, impinge the detectors within the coincidence time window of the system. Random coincidences also add statistical noise to the data.

The measurement of the time of flight (TOF) of the two 511 keV gammas recorded in coincidence in a PET scanner provides an effective way of reducing the background due to random coincidences and therefore increases the scanner sensitivity, provided that the coincidence resolving time (CRT) of the gammas is sufficiently good. Existing commercial systems based in LYSO crystals, such as the GEMINIS of Philips [1], reach CRT values of ~ 600 ps (FWHM).

Recent research, using small setups, has found much better results. For example Ferri et al. [2] report measurements using a pair of small LYSO crystals ($3 \times 3 \times 5$ mm^3)read out by high-fill factor SiPMs. With this setup, a CRT of 157 ± 5 ps was found at ambient temperature ($20\,^\circ$C). The CRT was considerably improved working at $-20\,^\circ$C, to a value of 125 ± 5 ps. The limiting factor of the CRT at ambient temperature was the impact of the dark current rate (DCR).

In this paper we present a Monte Carlo investigation of the CRT performance of a recently proposed new type of PET scanner, called PETALO (Positron Electron TOF Apparatus using Liquid xenOn). In section 2 we summarize the relevant properties of liquid xenon (LXe) as scintillating material and the main features of the PETALO scanner. In section 3 we review the mechanisms which produce scintillation light in LXe and propose a parameterization of the measured scintillation data in terms of two decay constants. In section 4 we discuss the CRT performance in LXe cells using SiPMs sensitive to the xenon ultraviolet light and conventional SiPMs coated with a suitable wavelength shifter. Conclusions are presented in section 5.

2   Liquid xenon as detection material and the PETALO concept

Physical properties of liquid xenon relevant for PET
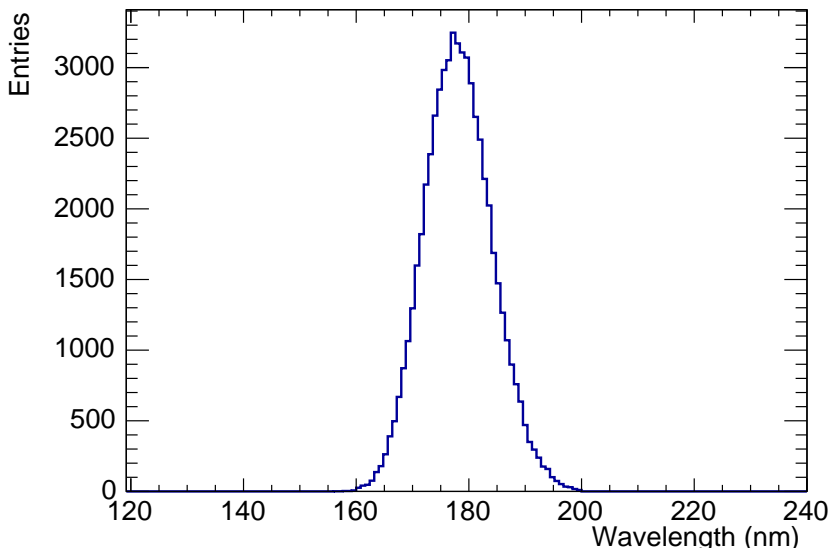
**Figure 1**.   Emission spectrum of scintillation photons in LXe.

Xenon is a noble gas. It responds to the interaction of ionizing radiation producing about 60 photons per keV of deposited energy. The emitted photons have wavelengths in the ultraviolet range (figure 1) with an average wavelength of 178 nm. The scintillation signal is fast (see section 3) and can thus result in an excellent CRT. In its liquid phase (at a temperature of $\sim$ 160 K and atmospheric pressure) LXe has a reasonable high density (3 g/cm^3) and an acceptable attenuation length (36 mm), which makes it suitable for PET applications. Its main attractive features are:

1. **A high scintillation yield (30 000 photons per 511 keV gamma)**, twice as large as that of LYSO.

2. **LXe is a continuous medium with uniform response**. The design of a compact system is much simpler, then, than when using solid detectors of fixed shape. It is also possible to provide a 3D measurement of the interaction point, and, thus, a high resolution measurement of the depth of interaction (DOI). Furthermore, in LXe it is possible to identify Compton events depositing all their energy in the detector as separate-site interaction, due to its relatively large interaction length. This increases the sensitivity of the system, since those events can, in principle, be used for image reconstruction.

3. **The temperature of LXe at atmospheric pressure (160 K or -113 C)** is hot enough as to permit a simple cryostat, as well as normal operation of the SiPMs, but cold enough to reduce the DCR of the SiPMs by a factor $\sim 2^{13}$, thus making it essentially negligible.

4. The cost of LXe is 3 $/cc to be compared with $\sim$ 40–50 $/cc in the case of LYSO.

The possibility of building a LXe PET based on the excellent properties of LXe as scintillator was first suggested by Lavoie in 1976 [3], and the study of this type of PET was carried out by the Waseda group [4–6]. The Waseda prototype was based in LXe cells read out by VUV-sensitive PMTs which covered 5 of the 6 sides of the cell.

PETALO

PETALO (Positron Electron TOF Apparatus using Liquid xenOn) is a proposed new type of PET scanner which exploits the copious scintillation of liquid xenon and the availability of state-of-the-art SiPMs and fast electronics designed to maximize TOF performance [7]. The detector building block is the liquid xenon scintillating cell (LXSC). The cell shape and dimensions can be optimised depending on the intended application. In particular, the LXSC2 instruments the entry and exit faces of the box (relative to the gammas line of flight) with silicon photomultipliers, while all the other faces are covered with a reflecting material such as Teflon (figure 2). They are read out by ASICs optimized for excellent timing resolution. PETALO is a compact, homogenous and highly efficient detector which shares many of the desirable properties of monolithic crystals, with the added advantage of high yield and fast scintillation offered by liquid xenon, low noise due to cryogenic operations which virtually eliminates the SiPMs DCR, and the potential of low cost.
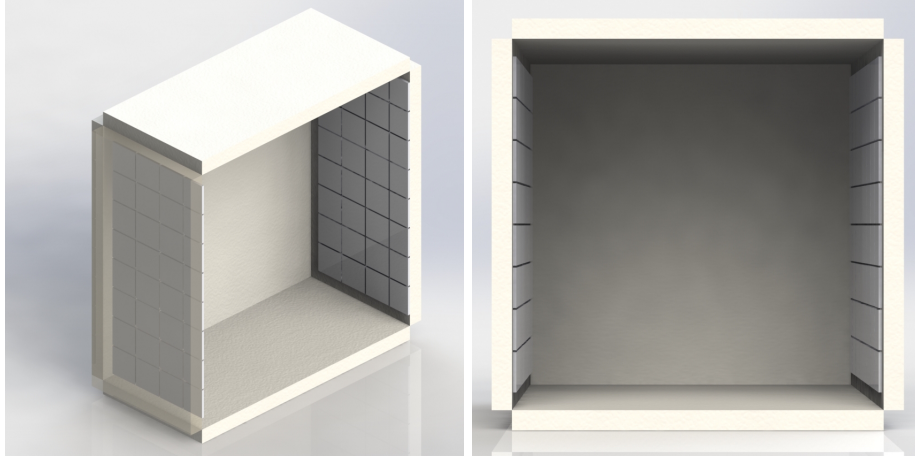
Figure 2. The LXSC2 instruments the entry and exit faces of the box (relative to the photon line of flight) with silicon photomultipliers (SiPMs), which can be eventually coated with TPB. The non-instrumented faces are covered by reflecting Teflon (optionally also coated with TPB).

The energy resolution R of a liquid xenon scintillation detector is a combination of light collection variation due to the detector geometry R_g, the statistical fluctuation of number of photoelectrons from the sensors R_s, the fluctuation of electron-ion recombination due to escape electrons R_r, and the intrinsic resolution from liquid xenon scintillation light R_i, due to the non-proportionality of scintillation yield, also associated to fluctuations in the number of secondary electrons. Therefore:

$$R^2 = R_g^2 + R_s^2 + R_r^2 + R_i^2 \tag{2.1}$$

The contribution of the intrinsic terms, (R_r and R_i) has been measured to be 11 % FWHM [8] for 511 keV gammas. The contribution of photoelectron statistics and geometrical effects for the LXSC2 configuration was found to be 3 % FWHM [7]. The combination of both effects yields an expected overall resolution of the order of 12% FWHM for 511 keV gammas, similar to that of LYSO detectors.

The spatial resolution in the (x,y) coordinates (transverse to the gammas line of flight) is obtained in the LXSC2 by the weighted pulses in the SiPMs. The digital resolution would be $p/\sqrt{12}$, where p is the pitch. With a pitch of 6 mm a 1.7 mm rms or 4 mm FWHM could be expected. Weighting with the SiPM amplitude improves the resolution to about 2 mm FWHM. The DOI is obtained by computing the ratio between the total signal recorded in the entry and exit face, and its resolution is found to be also 2 mm FWHM.

**VUV-sensitive SiPMs versus SiPMs coated with TPB**

The scintillation light of LXe peaks around 178 nm (VUV region). Therefore the LXSC2 needs to be instrumented either with VUV-sensitive SiPMs (as for example the upgraded LXe calorimeter of the MEG experiment [12]) or by conventional SiPMs coated with a wavelength shifter such as tetraphenyl butadiene (TPB) (as for example in the NEXT experiment [13]). The VUV-SiPMs tested for the MEG as well as for the future nEXO
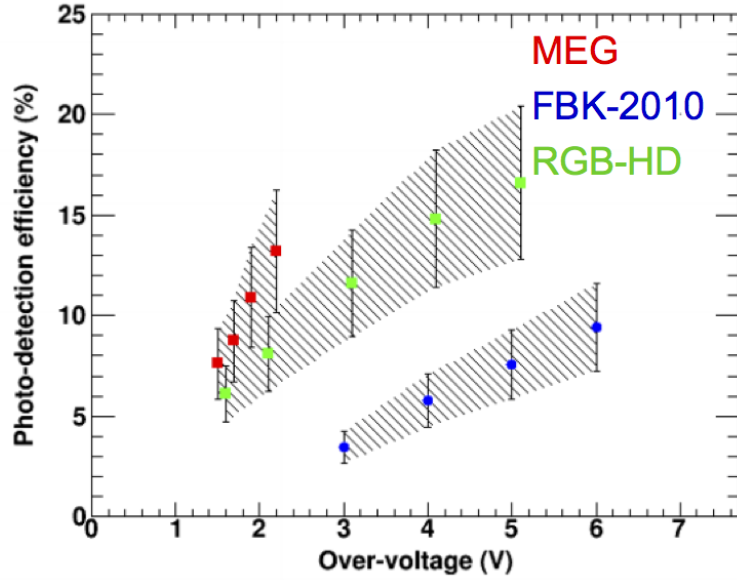
Figure 3. Photo detection efficiency (PDE) of different VUV sensitive SiPMs (from reference)[9]. The MEG devices are manufactured by Hamamatsu Photonics, while the FBK-2010 and the RGB-HD are manufactured by FBK.
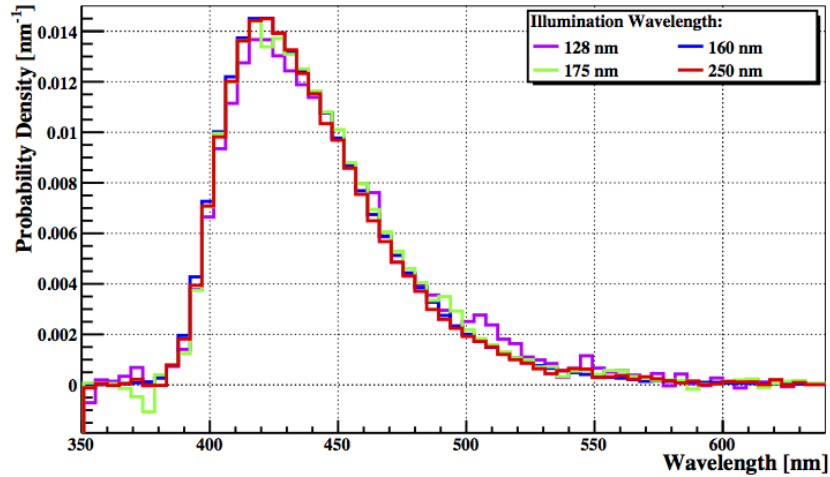
Figure 4. Visible re-emission spectrum for a TPB film illuminated with 128, 160, 175, and 250 nm light. All spectra are normalized to unit area. Figure from reference [10].
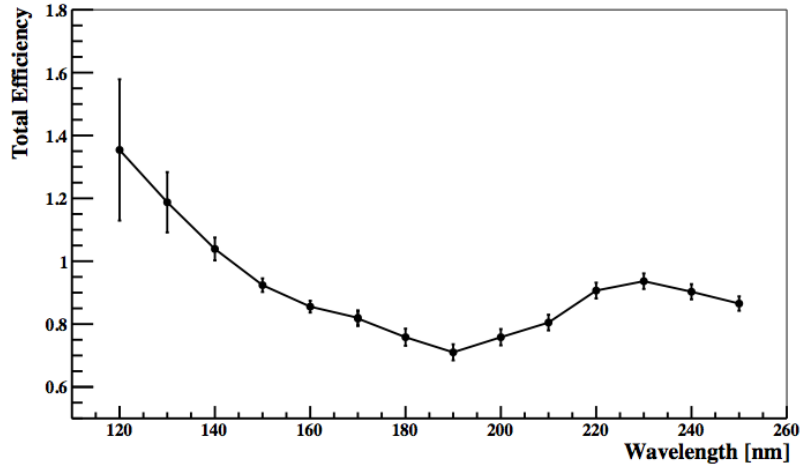
Figure 5. Total integrated fluorescence efficiency for a thin layer of TPB, as a function of input photon wavelength. Figure from reference [10].
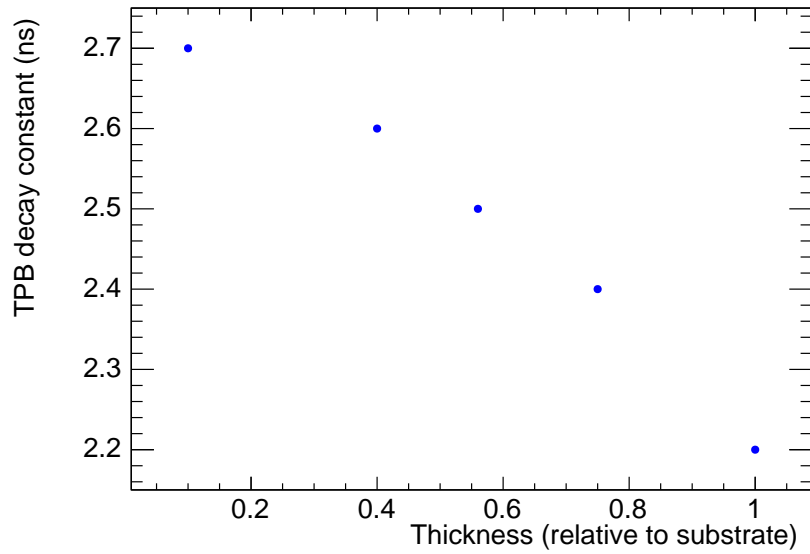
Figure 6. Evolution of the decay constant of TPB as a function of the thickness of the TPB layer compared with the thickness of the substrate (a thin quartz film). The TPB decay constant decreases as the thickness of the TPB layer (thus its concentration) increases, reaching an asymptotic value of 2.2 ns. Figure elaborated from reference [11].

experiment [12, 14] reach a PDE of about 15% (figure 3). Further improvements of the technology could eventually result in a PDE of 20%. Conventional SiPMs can reach today a PDE of around 50%. When they are coated with a thin layer of TPB, the VUV light is absorbed by the wavelength shifter with an efficiency of 80% [10] (figure 5) shifted to ~ 430 nm (figure 4) and re-emitted isotropically. The decay constant of TPB has been measured in thin films [11] and a value of 2.2–3 ns is found, depending on the TPB concentration (see figure 6). For sufficiently large TPB concentrations, the decay constant may be of the order of 1–2 ns.

3 Scintillation in LXe

When a 511 keV gamma interacts in liquid xenon it will produce a secondary electron (by either photoelectric or Compton interaction) which in turn will propagate a short distance in the liquid, ionizing the medium. Most of the scintillation light in xenon is emitted by diatomic excited molecules which are formed through two distinct processes:

1. Excitation of atoms by electron impact with subsequent formation of strongly bound diatomic molecules in the excited state (excitons). We refer to this process as scintillation due to exciton self-trapping or SE.

2. Recombination of the ionization electrons with positive ions. We call this process scintillation due to recombination or SR.

Both processes are very fast (of the order of the ps) and therefore scintillation in LXe does not have a physical rise constant. The two decay constants are related with the decay of the two lowest excited molecular states $({}^1\Sigma_u^+, {}^3\Sigma_u^+)$. The decay of the singlet state $({}^1\Sigma_u^+)$ occurs with a lifetime $\tau_1 = 2.2$ ns, while the lifetime of the triplet state $({}^3\Sigma_u^+)$ is $\tau_2 = 27$ ns.

The relative contribution of SE and SR processes to the LXe scintillation light has been measured to be [15]:

$$I = 0.3 \times I^S + 0.7 \times I^R \tag{3.1}$$

where I^S refers to the intensity of the SE process and I^R to the intensity of the SR process.

Also, after the measurements in reference [15], I^S and I^R can be written as:

$$I^S = 0.15 \times I_1^S(t) + 0.85 \times I_2^S(t) \tag{3.2}$$
$$I^R = 0.44 \times I_1^R(t) + 0.56 \times I_2^R(t) \tag{3.3}$$

The time dependence of the SE process is described by:

$$I_i^S = \frac{e^{-t/\tau_i}}{\tau_i} \tag{3.4}$$

where $i = 1, 2$. The time dependence of the RE process is more complicated, since the recombination time T_r of the electrons is slow compared with the fast constant τ_1. Then, I_1^R can be parameterized [15] as:

$$I_1^R = (1 + \frac{t}{T_r})^{-2} \tag{3.5}$$

where $T_r \sim 15$ ns for xenon. Instead, since $\tau_2 > T_r$, I_2^R can be described as in the case of the SE processes:

$$I_2^R = \frac{e^{-t/\tau_2}}{\tau_2} \tag{3.6}$$
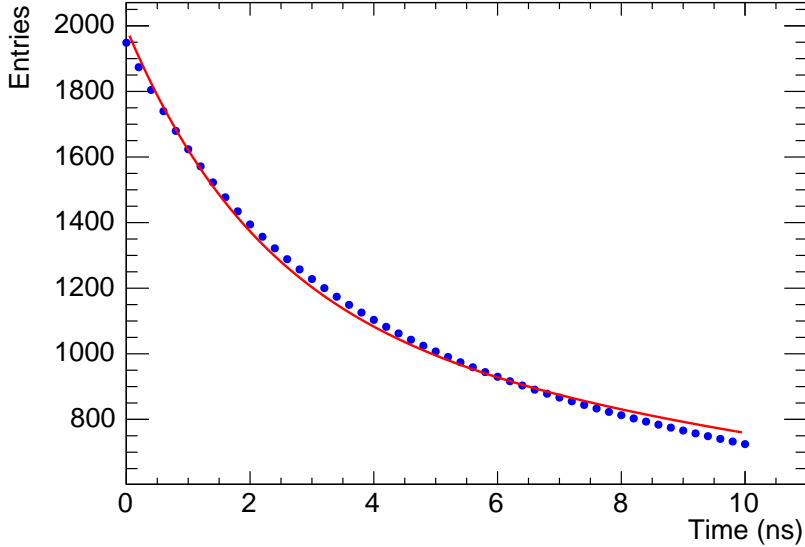
Figure 7. Intensity of scintillation in LXe, fitted to equation 3.

Figure 7 shows the total intensity of scintillation in LXe for a 511 keV gamma (resulting in a total of $N_\gamma = 30\,000$ VUV photons), adding the contribution of SE and SR processes (blue dots). This distribution is well described in terms of the sum of two exponential distributions with decay constants τ_1 and τ_2. The fit, shown in figure 7, gives the following distribution for the number of photons:

$$I(t) = N_\gamma(0.07 \times \frac{e^{-t/\tau_1}}{\tau_1} + 0.93 \times \frac{e^{-t/\tau_2}}{\tau_2}) \tag{3.7}$$

Equation 3.7 fits better in the short range, which is the most relevant for CRT estimations.

4 Monte Carlo study of the CRT in the LXSC2

To systematically study the different factors that enter the CRT, we have simulated a LXe setup and a LYSO setup, using the Geant-4 toolkit [16]. The LXe setup consists of two LXSC2 of $2.4 \times 2.4 \times 5$ cm^3, facing each other in opposite sides of a 511 keV gamma source (figure 8) and equipped with SiPMs which can be either sensitive to the xenon ultraviolet (VUV) light, or coated with a wavelength shifter such as tetraphenyl butadiene (TPB). The

LYSO setup replaces the two LXe cells by a pair of monolithic LYSO crystals of identical dimensions, also read out by SiPMs.
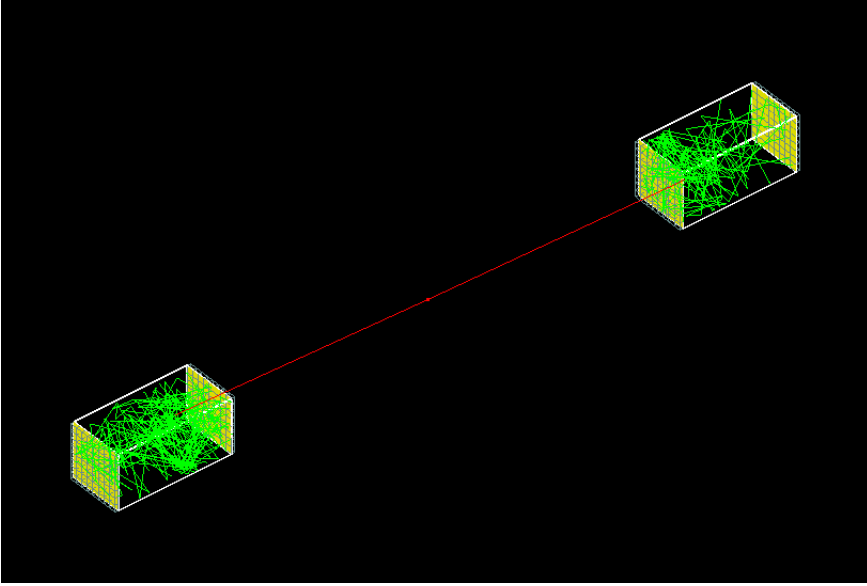

Figure 8. Monte Carlo simulation of gamma interactions in the LXe setup, as described in the text.

Back to back 511 keV gammas are shot isotropically, from a common vertex within the solid angle covered by two opposite LXSC2 ($2.4 \times 2.4 \times 5$ cm^3). The gammas fly a distance dg_1, dg_2 before interacting in the LXSCs. Scintillation photons are produced according to equation 3.7 for LXe (in the case of LYSO they are produced according to a single decay constant of 40 ns) and propagated through the material. The photons reach eventually the SiPMs. If the SiPM is not coated with TPB, the photon will enter the SiPM window if the angle of incidence is below the critical angle defined by the ratio of the refraction indexes of the LXSC (LYSO) and the SiPM window $\sin \theta_c = n_2/n_1$, where we take $n_1 = 1.54$ as the refraction index of the SiPM window and $n_2 = 1.7(1.8)$ as the refraction index of the LXe (LYSO). If the SiPM is coated with TPB, the VUV photon is absorbed with an efficiency of 80% and re-emitted isotropically with a wavelength given by figure 4, then enters the SiPM window with a much larger critical angle, since $n_2 = 1.55 \sim n_1$ for LXe in the visible region. Depending on the PDE of the SiPM the incident photon may result in a photoelectron. Denoting t_1, t_2 as the time of the first photoelectron recorded in each one of the LXSC, the time difference between them can be written as:

$$\Delta t = \frac{1}{2}(t_2 - t_1 - \frac{\Delta d_g}{c} - \frac{n \cdot \Delta d_p}{c}) \tag{4.1}$$

where $\Delta d_g/c$ is the time of flight difference from the emission to the interaction vertex of the two 511 keV gammas, and $n \cdot \Delta d_p/c$ is the time of flight difference from the interaction vertex to the detection vertex (e.g, the position of the sensor) of the scintillation photons.

The CRT, $\delta\Delta t$, is defined as the variance[1] of the Δt distribution.
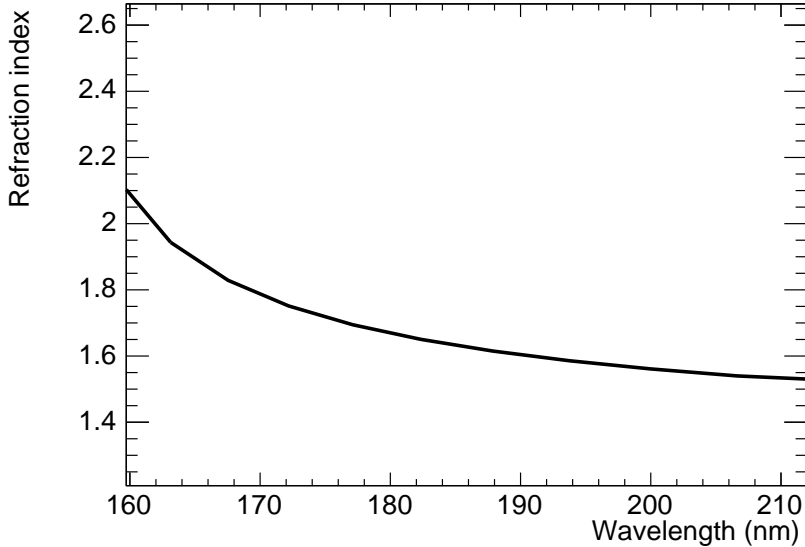
Figure 9. LXe refraction index as a function of the wavelength of the optical photon.

Notice that, while the calculation of the term $\Delta d_g/c$ is immediate, finding the value of $n \cdot \Delta d_p/c$ requires the knowledge of the refraction index of the medium (which in turn is a function of the wavelength of the scintillation photons, see figure 9) and the interaction vertices of the gammas in the LXSCs, whose determination depends on the spatial resolution (and in particular of the DOI resolution) of the setup. Furthermore, the recorded time of the photoelectrons is affected by the time jitter of the sensor and the front-end electronics, as well as by the overall clock system. Other effects that affect the CRT are the existence of a rise constant for scintillation (absent in the case of LXe, but of the order of 70 ps for LYSO [17]), and the additional decay constant (about 2.2 ns) introduced if the SiPMs of the LXSC2 are coated with TPB.

In the remaining of this section we study systematically the various factors contributing to the CRT in LXe.

Intrinsic CRT: effect of the DOI resolution

We start our study by assuming that the refraction indices in both media are constant, with values 1.7 for LXe and 1.8 for LYSO. We also fix the refraction index of the SiPM window to the same value of the propagation medium (LXe or LYSO, depending on the setup), so that $n_1 = n_2$ and therefore all photons impinging the SiPM with an angle less than $90°$ enter the sensor. This (unphysical) assumptions are made in order to separate the contributions to the CRT due to the scintillation lifetime and the DOI resolution from those related with the refraction index.

Figure 10 shows the arrival time of the first photoelectron in LXe and LYSO, after subtracting the time of flight of the incident gamma ($\Delta d_g/c$) and the time of flight of

---

[1]expressed in number of FWHM unless explicitly stated otherwise.
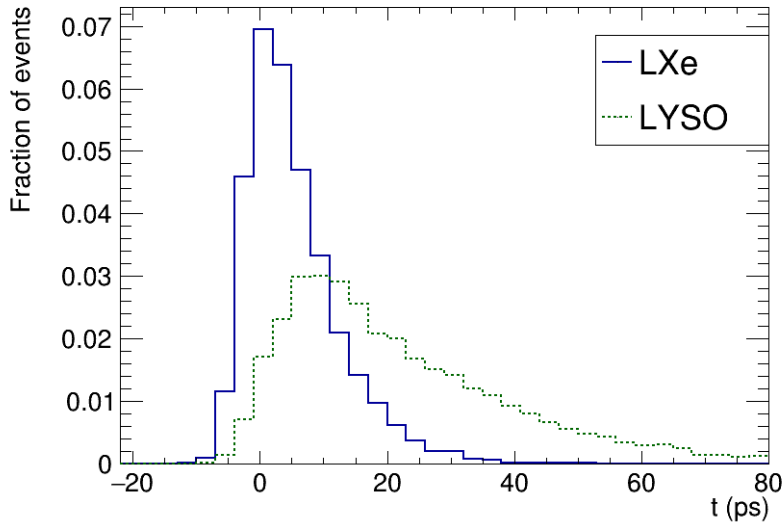
Figure 10. Arrival time of the first photoelectron in LXe (blue line) and LYSO (green dotted), after subtracting the time of flight of the incident gamma ($\Delta d_g/c$) and the time of flight of the scintillation photons ($n \cdot \Delta d_p/c$).

the scintillation photons ($n \cdot \Delta d_p/c$). As expected, given the faster decay time, the VUV photons emitted by LXe arrive to the sensors earlier (and with a narrower distribution) than the blue photons emitted by LYSO.

Notice that Δd_p is the difference between the position of the interaction vertex and the position of the SiPM which records the photoelectron. The plot is computed introducing a resolution of 2 mm FWHM both in the transverse coordinates and in the DOI (which corresponds to the resolution expected in the LXSC2). The jitter introduced by the DOI correction is:

$$\delta\Delta t = \Delta z \times (n - 1) \times 3.3 \text{ ps/mm} \qquad (4.2)$$

For LXe, with n = 1.7, $\delta\Delta t = 4.4$ ps, while for LYSO, with n = 1.8, $\delta\Delta t = 5.4$ ps in both cases for a DOI resolution $\Delta z = 2$ mm. The effect is, therefore, small. Notice, on the other hand, that a DOI resolution of 2 mm FWHM requires either a double layer of SiPMs (as in the LXSC2) or small monolithic crystals (for example, in reference [18] the authors find a DOI resolution varying between 1 and 4.5 mm FWHM for LYSO crystals of $20 \times 20 \times 12$ mm^3)). Instead, a conventional segmented LYSO crystal, 20 mm thick, would have a DOI resolution of $2.3 \times 20\text{mm}/\sqrt{12} = 5.8$ mm, thus 13.3 mm, resulting in a $\delta\Delta t = 35.2$ ps.

Figure 11 shows $\delta\Delta t$ for LXe and LYSO for the ideal case of PDE = 1. The wider LYSO distribution is due to the slower decay constant. Figure 12 shows the CRT as a function of the SiPM PDE. The CRT of the LXe setup for PDE=1 is ~10 ps, while the intrinsic resolution of the LYSO setup for PDE=1 is ~30 ps. This values can be taken as the absolute best limit of the CRT in LXe and LYSO. For a PDE of 50%, (best value of
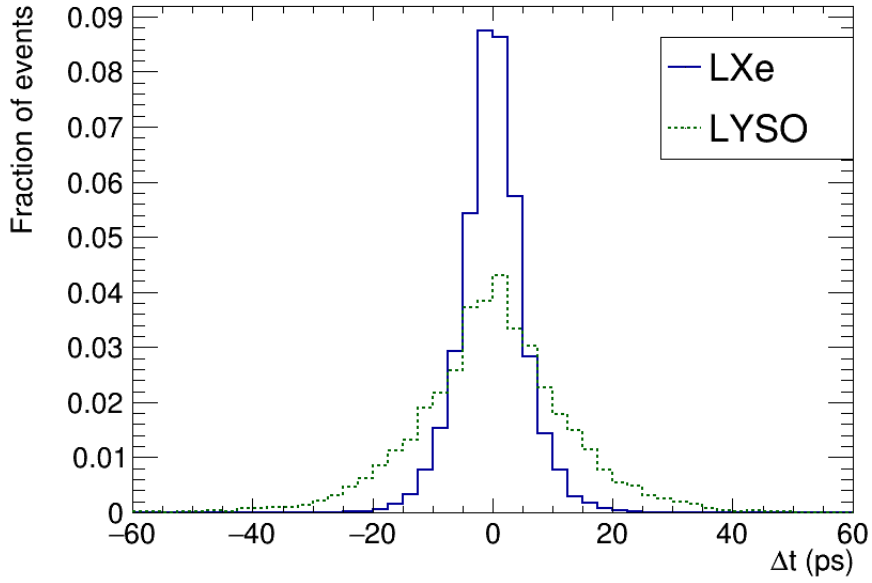
Figure 11. $\delta\Delta t$ in LXe (blue line) and LYSO (green dotted line). The histograms are obtained introducing a spatial resolution of 2 mm for the transverse coordinates and the DOI, fixing the wavelength of the scintillation and the refraction index and setting the PDE of the SiPMs to one.
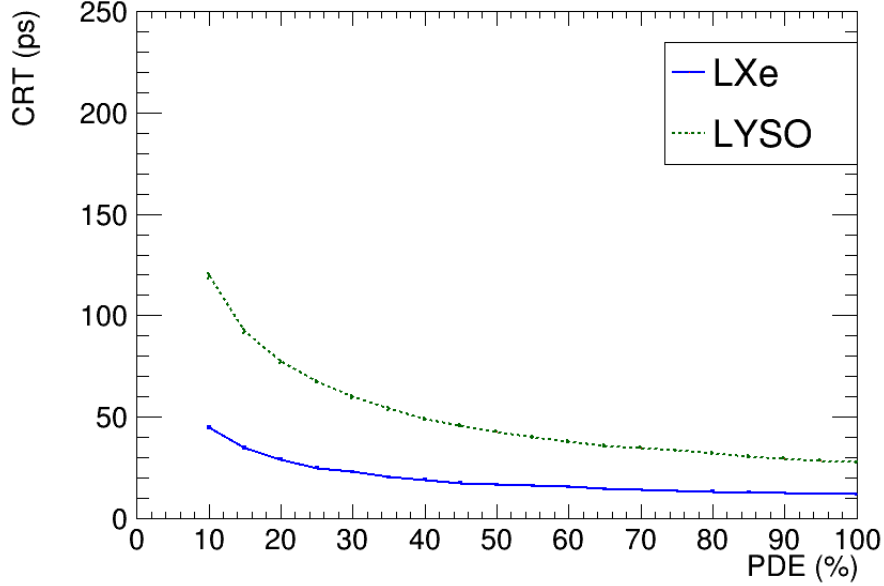
Figure 12. CRT as a function of the PDE in LXe (blue line) and LYSO (green dotted line) computed using the first photoelectron. The calculation takes into account the scintillation yield and decay time as well as the DOI resolution but does not include the dependence of the refraction index in LXe with wavelength.

conventional SiPMs) the CRT in LYSO is ~ 45 ps, while for a PDE of 20% (best value of VUV–sensitive SiPMs) the CRT in LXe is ~ 30 ps.

Effect of the refraction index
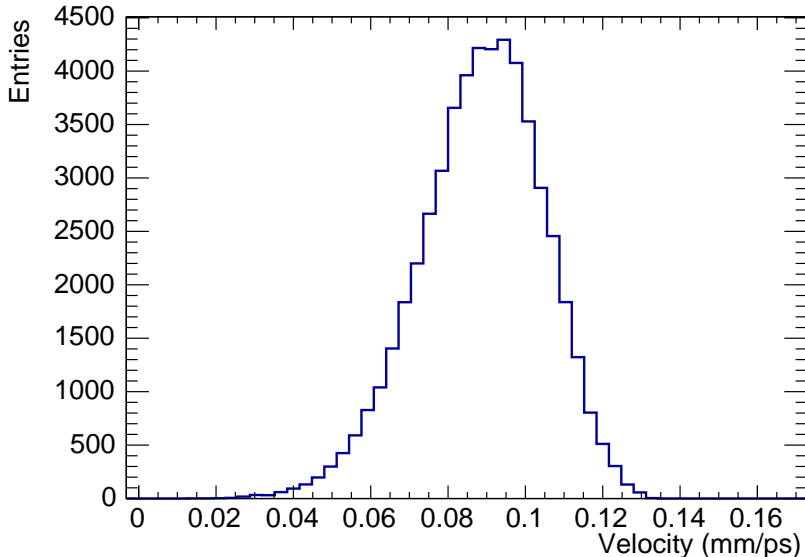
Figure 13. Distribution of the velocity of scintillation photons propagating in LXe.

The refraction index in LXe varies significantly with the scintillation photon wavelength, as shown in figure 9 (instead, the refraction index of LYSO is practically constant in the relevant range of scintillation emission). This implies that the xenon VUV photons propagate with different velocities depending of their wavelength, as shown in figure 13. To take into account this effect, one must use the average group velocity of the photons instead of the constant term n/c in equation 4.1. This introduces an extra smearing which contributes to the CRT, due to the spread of the average velocity.

We also introduce the refraction index of the SiPM entrance window, which we take as $n_1 = 1.54$ (a typical value, quoted, for example for the SensL C-series 6 mm sensors). The mismatch with the xenon refraction index ($n_2 \sim 1.7$ in the VUV region) or the LYSO refraction index ($n_2 = 1.8$) results in a reduction of the efficiency due to Fresnel reflections. The critical angle in xenon is 65° (58° in LYSO) and the fraction of photons transmitted through the SiPM window is 63.5% for LXe (56% for LYSO).

Figure 14 shows the CRT as a function of the SiPM PDE when the effect of the refraction index is taken into account. The effect of the variable refraction index deteriorates considerably the intrinsic CRT in LXe, resulting in a value of $\sim$27 ps for PDE=1 while it has little effect in LYSO. The CRT in LXe for a PDE of 20% and in LYSO for a PDE of 50% is ~ 50 ps.
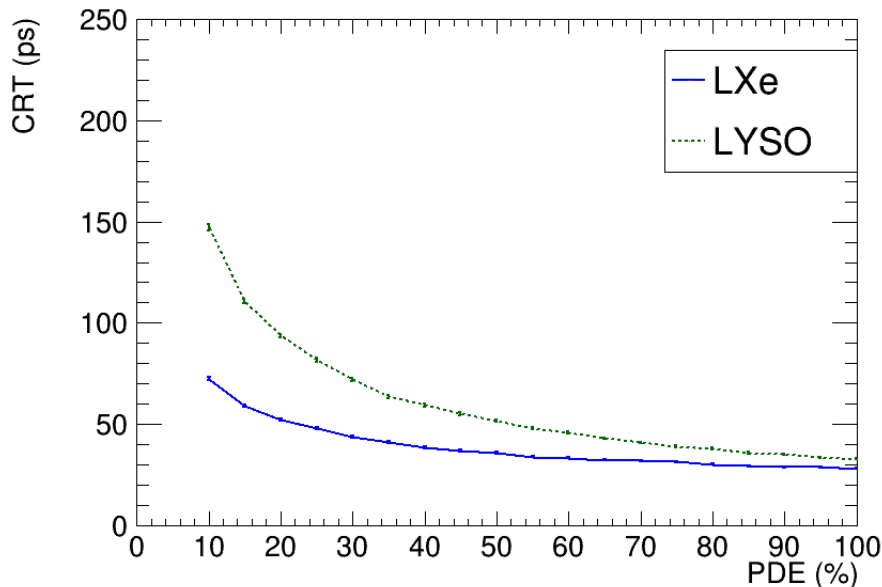
Figure 14. CRT as a function of the PDE in LXe (blue line) and LYSO (green dotted line) computed using the first photoelectron. The calculation takes into account the scintillation yield and decay time as well as the DOI resolution and the dependence of the refraction index in LXe with wavelength. The effect of Fresnel reflections due to the mismatch between the LXe (LYSO) refraction index and that of the SiPM is also taken into account.
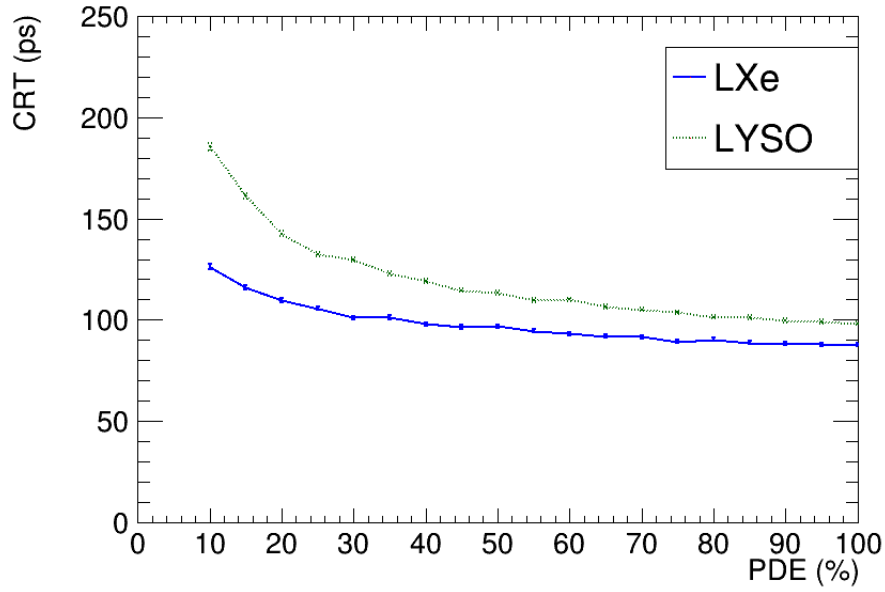
Effect of the SiPM and front-end electronics jitter

Next we introduce the effect of the jitter of the SiPM and front-end electronics, smearing the arrival time of the photoelectrons by a gaussian distributions with $\sigma = \sigma_{sipm} + \sigma_{fee}$ and setting $\sigma_{sipm} = 80$ ps, $\sigma_{fee} = 30$ ps. These values are typical of modern SiPMs and front-end electronics [19].
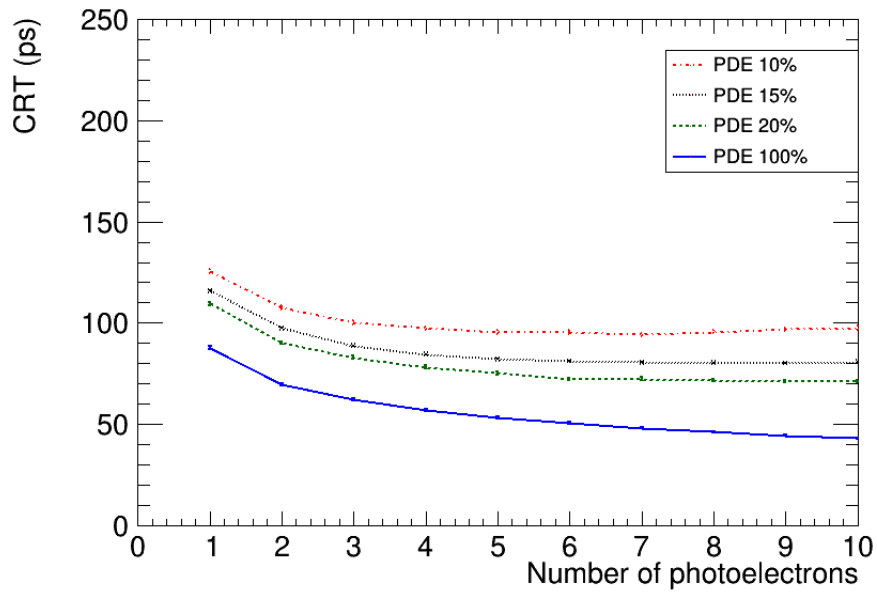
Figure 15 shows the CRT as a function of the SiPM nominal PDE for LX (red curve) and LYSO (green curve). The CRT includes the for $PDE = 1$ is 90 ps for LXe and 100 ps for LYSO. For a PDE of 50% the CRT in LYSO is ~ 125 ps, while for a PDE of 20% the CRT in LXe is ~ 100 ps. However, the CRT can improve computing Δt as an average of the first few photoelectrons, rather than using only the first photoelectron. This is shown in figures 16 and 17. For a PDE of 20%, it appears possible to reach a CRT of 70 ps in the case of LXe, and about 85 ps in LYSO for a PDE of 50%.

Interestingly, the results obtained for LYSO using the first photoelectron to compute Δt (a CRT of 125 ps for a PDE of 50%), agree rather well with the results of Ferri et al [2] *when the LYSO crystals were cooled to* $-20\,°C$, e.g, reducing the DCR by a factor 16). The obvious advantage of LXe is the cryogenic operation, at $\sim -100\,°C$, which essentially eliminates the effect of the DCR. Thus, an excellent CRT of 70 ps could be achieved if the SiPM–VUV technology is capable of producing sensors with a PDE of 20%. For a PDE of 15% corresponding to the best existing devices, the CRT averaging over several photoelectrons is 80 ps, still very good.
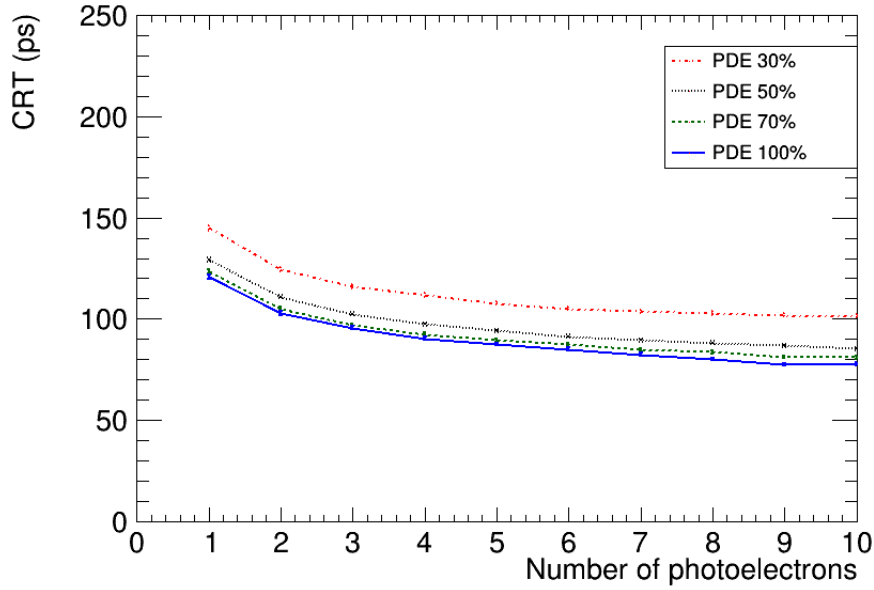
Figure 15. CRT as a function of the PDE in LXe (blue line) and LYSO (green dotted line) computed using the first photoelectron. The calculation includes the effect of the SiPM and front-end electronics jitter.
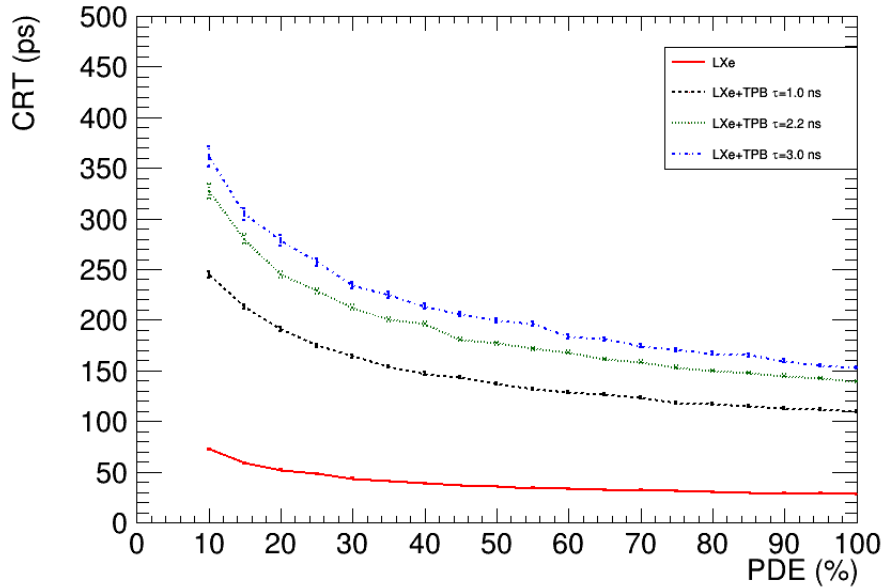

Figure 16. CRT as a function of the number of photoelectrons used to compute Δt, for LXe. The CRT is shown for several values of the PDE.
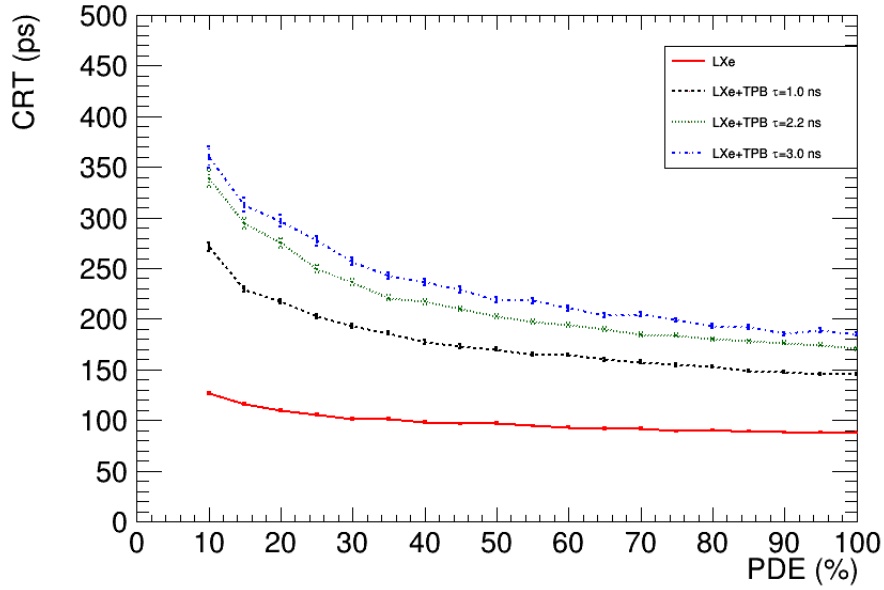
Figure 17. CRT as a function of the number of photoelectrons used to compute Δt, for LYSO. The CRT is shown for several values of the PDE.

Effect of the TPB decay constant

Figure 18. CRT as a function of the PDE in LXe (red line) and LXe coated with TPB, assuming several decay times. The CRT is computed using the first photoelectron. The calculation takes into account the scintillation yield and decay time as well as the DOI resolution and the dependence of the refraction index in LXe with wavelength.

We now consider the case in which conventional SiPMs, with a PDE as large as 50%

Figure 19. CRT as a function of the PDE in LXe (red line) and LXe coated with TPB, assuming several decay times. The CRT is computed using the first photoelectron. The effect of the jitter of the SiPM and electronics is included.

in the blue region, are used in a PETALO scanner. The SiPMs would be coated with TPB to shift the VUV light to blue. The main reason to consider this scenario is cost. VUV sensitive SiPMs are currently much more expensive (up to a factor of 10) than conventional SiPMs. It must be pointed out that such a cost difference can be quickly reduced with technological advances and massive production. Nevertheless, a PETALO scanner using TPB–coated SiPMs could be built with existing technology at a very competitive cost and is, therefore, interesting to study the effect of TPB on the CRT.

Figure 18 shows the CRT as a function of the SiPM nominal PDE for VUV sensitive SiPMs and TPB-coated SiPMs in LXe. The calculation takes into account the scintillation yield and decay time as well as the DOI resolution and the dependence of the refraction index in LXe with wavelength, but not the jitter due to the SiPM and electronics. Here we must compare the CRT achieved for VUV sensitive SiPMs with a PDE of 15–20% ($\sim$ 50 ps) with the CRT achieved for blue sensitive SiPMs coated with TPB, taking as a reference a PDE of 50% (this corresponds to the PDE for blue light, however, the CRT is computed taking into account the effect of the TPB absorption and subsequent re-emission). The CRT in this case varies from 140 ps (for a decay constant $\tau_{\mathrm{TPB}} = 1$ ns) to 200 ps (for a decay constant $\tau_{\mathrm{TPB}} = 3$ ns). When the effect of the jitter of the SiPM and front-end electronics is added (figure 19), the CRT (first photoelectron) for VUV-SiPMs is $\sim$ 100 ps, while the CRT for TPB-coated SiPMs varies from 170 ps (for a decay constant $\tau_{\mathrm{TPB}} = 1$ ns) to 220 ps (for a decay constant $\tau_{\mathrm{TPB}} = 3$ ns). Averaging Δt over the first 10 photoelectrons the CRT is reduced to 130 ps for a decay constant $\tau_{\mathrm{TPB}} = 1$ ns; 155 ps for a decay constant $\tau_{\mathrm{TPB}} = 2.2$ ns; and 170 ps for a decay constant $\tau_{\mathrm{TPB}} = 3$ ns. Notice that averaging over several photoelectrons reduces the error in the CRT by a large factor in the case of SiPMs

coated with TPB.

The results obtained with TPB are still very good. The best case scenario corresponds to a decay time of 1 ns (which can arguably be obtained with a thick enough coating) and yields a CRT of 130 ps, comparable to the value obtained by Ferri et al [2] when the LYSO crystals were cooled to $-20\,^{\circ}$C.

5 Summary and outlook

We have studied the CRT that can be obtained by a PETALO scanner based in the LXSC2 cell. The intrinsic resolution of the cell (corresponding to an ideal VUV sensitive sensor of PDE one and forcing a fixed refraction index) is 12 ps, of which DOI uncertainty contributes with about 5 ps. Introducing a PDE of 15%, corresponding to the best currently achieved by VUV-sensitive SiPMs, still results in an excellent CRT of 35 ps. Including the effect of the variable refraction index and Fresnel reflections, a CRT of 55 ps is found for a PDE of 15%. Adding the effect of the jitter of the SiPM and electronics spoils the CRT to some 115 ps for a PDE of 15%. Averaging Δt over the first few photoelectrons, one recovers a CRT of 80 ps for a PDE of 15% and 70 ps for a (technically feasible) PDE of 20%. It follows that a PETALO scanner based in the LXSC2 cell equipped with VUV sensitive SiPMs of relatively large PDE (15% or better) could reduce the CRT of a large system well below the 100 ps threshold.

On the other hand, we find that using blue sensitive SiPMs coated with TPB results in a CRT that could be as good as 130–155 ps (for $\tau_{\mathrm{TPB}} = 1 - 2.2$ ns). These values still compete with the best results obtained for LYSO. In summary, it appears feasible to build a PETALO scanner with existing technology, combining the advantages of large sensitivity (due to increased large axial acceptance afforded by the low cost of xenon compared with LYSO), good energy and spatial resolution, and excellent CRT.

References

[1] S. Surti *et al.*, "Performance of Philips Gemini TF PET/CT Scanner with Special Consideration for Its Time-of-Flight Imaging Capabilities," *J. Nucl. Med.* , vol. 48, pp. 471–480, 2007.

[2] A. Ferri, A. Gola, N. Serra, A. Tarolli, N. Zorzi, and C. Piemonte, "Performance of FBK high-density SiPM technology coupled to Ce:LYSO and Ce:GAGG for TOF-PET," *Phys. Med. Biol.*, vol. 59, pp. 869–880, 2014.

[3] L. Lavoie, "Liquid xenon scintillators for imaging of positron emitters," *Medical Physics 3*, vol. 5, p. 283, 1976.

[4] T. Doke, J. Kikuchi, and F. Nishikido, "Time-of-flight positron emission tomography using liquid xenon scintillation," *Nucl. Instrum. Methods A*, vol. 569, p. 863, 2006.

[5] F. Nishikido *et al.*, "Performance of prototype liquid xenon scintillation detector system for Time-of-Flight Type Positron Emission Tomography with improved photomultipliers," *Japanese Journal of Applied Physics*, vol. 44, p. 5193, 2005.

[6] F. Nishikido *et al.*, "Performance of a Prototype of Liquid Xenon Scintillation Detector System for Positron Emission Tomography," *Japanese Journal of Applied Physics*, vol. 43, p. 779, 2004.

[7] J. J. Gomez-Cadenas, J. M. Benlloch-Rodriguez, and P. Ferrario, "Application of scintillating properties of liquid xenon and silicon photomultiplier technology to medical imaging," *Spectrochimica Acta*, vol. 118, pp. 6–13, Apr. 2016.

[8] K. Ni, E. Aprile, K. Giboni, P. Majewski, and M. Yamashita, "Gamma Ray Spectroscopy with Scintillation Light in Liquid Xenon," *JINST*, vol. 1, p. P09004, 2006.

[9] C. Rethmeier, "Characterization of VUV sensitive SiPMs for nEXO." http://neutrino.physics.ucdavis.edu/indico/getFile.py/access?contribId=61&sessionId=2&resId=0&materialId=slides&confId=17.

[10] V. M. Gehman, S. R. Seibert, K. Rielage, A. Hime, Y. Sun, D. M. Mei, J. Maassen, and D. Moore, "Fluorescence Efficiency and Visible Re-emission Spectrum of Tetraphenyl Butadiene Films at Extreme Ultraviolet Wavelengths," *Nucl. Instrum. Meth.*, vol. A654, pp. 116–121, 2011.

[11] J. Huang, V. Bekiari, P. Lianosa, and S. Couris, "Study of poly(methyl methacrylate) thin films doped with laser dyes," *Journal of Luminescence*, vol. 81, no. 4, pp. 285–291, 1999.

[12] S. Ogawa, "Upgrade of liquid xenon calorimeter in MEG experiment with VUV sensitive MPPCs," *PoS*, vol. FPCP2015, p. 063, 2015.

[13] V. Álvarez *et al.*, "Operation and first results of the NEXT-DEMO prototype using a silicon photomultiplier tracking array," *JINST*, vol. 8, p. P09011, 2013.

[14] I. Ostrovskiy *et al.*, "Characterization of Silicon Photomultipliers for nEXO," *IEEE Trans. Nucl. Sci.*, vol. 62, p. 1825, 2015.

[15] S. Kubota, M. Hishida, M. Suzuki, and J. Ruan, "Dynamical behaviour of free electrons in the recombination process in liquid argon, krypton and xenon," *Physical Review B*, vol. 20, p. 8, 1979.

[16] S. Agostinelli *et al.*, "Geant4: A Simulation toolkit," *Nucl. Instrum. Meth. A*, vol. 506, pp. 250–303, 2003.

[17] S. Seifert, "Accurate measurements of the rise and decay times of fast scintillators with solid state photon counters," *Nuclear Science Symposium Conference Record (NSS/MIC)*, pp. 1736 – 1739, 2010.

[18] H. T. Van Dam, S. Seifert, R. Vinke, P. Dendooven, H. Lohner, F. J. Beekman, and D. R. Schaart, "A practical method for depth of interaction determination in monolithic scintillator PET detectors," *Phys. Med. Biol.*, vol. 56, pp. 4135–4145, 2011.

[19] E. Derenzo, C. Woon-Seng, and N. W. Moses, "Fundamental Limits of Scintillation Detector Timing Precision," *Phys Med Biol.*, vol. 59, no. 13 345, pp. 3261–3286, 2014.